

## Article

# Residual Stresses on Various PVD Hard Coatings on Tube and Plate Substrates

Harri Lille <sup>1</sup>, Alexander Ryabchikov <sup>1,\*</sup>, Priidu Peetsalu <sup>2</sup>, Liina Lind <sup>2</sup>, Fjodor Sergejev <sup>2</sup>, Valdek Mikli <sup>3</sup> and Jakob Kübarsepp <sup>2</sup> 

<sup>1</sup> Institute of Forestry and Rural Engineering, Estonian University of Life Sciences, Kreutzwaldi 5, 51006 Tartu, Estonia; harri.lille@emu.ee

<sup>2</sup> Department of Mechanical and Industrial Engineering, Tallinn University of Technology, Ehitajate tee 5, 19086 Tallinn, Estonia; priidu.peetsalu@taltech.ee (P.P.); liina.lind@taltech.ee (L.L.); fjodor.sergejev@taltech.ee (F.S.); jakob.kubarsepp@taltech.ee (J.K.)

<sup>3</sup> Department of Materials and Environmental Technology, Tallinn University of Technology, Ehitajate tee 5, 19086 Tallinn, Estonia; valdek.mikli@taltech.ee

\* Correspondence: alexander.ryabchikov@emu.ee

Received: 24 September 2020; Accepted: 27 October 2020; Published: 30 October 2020



**Abstract:** In this study, the average residual stresses were determined in hard PVD nACRo (nc-AlCrN/a-Si<sub>3</sub>N<sub>4</sub>), nACo (nc-AlTiN/a-Si<sub>3</sub>N<sub>4</sub>), AlCrN, TiAlN, and TiCN commercial coatings through the deflection of the plate substrates and the simultaneous measurement of length variation in thin-walled tubular substrates. The length measuring unit was used for the measurement of any length change in the tubular substrate. A change in tube length was reduced to the deflection of the middle cross-section of the elastic element for which deformation was measured using four strain gauges. The cross-sectional microstructure and thickness of the coatings were investigated by means of scanning electron microscopy (SEM), and a determination was made of the chemical composition of the coatings and substrate by means of energy dispersive X-ray spectroscopy (EDS). The values of average compressive residual stresses, as determined by both methods, were very high (with a variation of between 2.05 and 6.63 GPa), irrespective of coating thickness, but were dependent upon the shape of the substrate and on its position in relation to the *axis* of the rotating cathode. The thicknesses of the coatings that were deposited on the plates with two parallel fixings (such as the nACRo coatings on the front surface at 6.8 μm and on the rear surface at 2.9 μm) and on the tubular substrates (10.0 μm) were significantly different. The higher average compressive residual stresses in the coating correlate to the higher average relative wear resistance that was obtained during field wear testing.

**Keywords:** PVD coatings; nACRo; nACo; AlCrN; TiAlN; TiCN; residual stresses; tube length variation; curvature method; indentational surface fatigue; industrial field wear tests

## 1. Introduction

Physical Vapor Deposition (PVD) coatings are used inter alia for blanking, punching, and cutting applications [1] and can be deposited both on plain surfaces and more complex ones [2,3]. It is well known that residual stresses that arise in coatings during the deposition process [1,4,5] have an important effect on the service life of the coating by means of influencing its mechanical and tribological properties and adhesion [6]. In general, residual macro- and microstresses in materials can be distinguished. Macro stresses (average values), as Type I, vary within a bulk coating, and micro stresses, as Type II, operate at the grain-sized level [7,8].

It should be noted that the (micro) residual stresses that have been measured by X-ray diffraction are the arithmetic average stress results in the small irradiated area alone. To be able to gain residual

[illegible]

The PVD coatings being studied were produced at the Material Engineering Research Centre, Tallinn University of Technology. The PVD unit, a Platit  $\pi$ -80 with Lateral Rotating ARC-Cathode technology, and with two rotating cathodes embedded in the door of the vacuum chamber, was used for deposition. The commercial coatings being used were deposited on specimens whose roughness was similar to that of cutting tools. A schematic for the placement of specimens in the vacuum chamber is presented in Figure 1. The tubes had two different wall thicknesses (outer diameter  $d_1 \times$  inner diameter  $d_2 \times$  length), shown as Tube 1 (3.0 mm  $\times$  2.70 mm  $\times$  167.37 mm) and Tube 2 (3.0 mm  $\times$  2.50 mm  $\times$  167.57 mm), and these were affixed vertically within the rotary table (which had a rotational speed of 12 rpm) inside the vacuum chamber. To prevent the coating being deposited on the cross-section of the tube ends, they were closed off at the nozzle, so that the entire outer surface of the tube could be coated [11]. At the same time, the tube was vertically fixed by the lower nozzle to the rotary table in the deposition chamber, and it was simultaneously rotated around its *axis* (Figure 1).

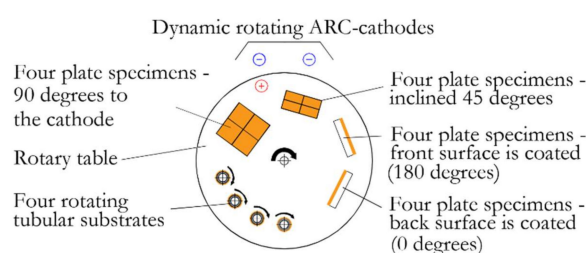


**Figure 1.** Schematic showing the placement of specimens in relation to the cathode in the vacuum chamber.

As the cutting edge of the cutting tools in the deposition chamber are placed at different angles, four placement angles were used with respect to the cathode during coating deposition. The plates are only deposited on one side and should be placed so that they are gripped by a claw in the affixing unit, which should be made of carbon steel (adapted from [10]). Note that a considerable amount of the evaporated target material was also deposited on the holder. Four plates were mounted on the holder so that one batch of the plates could be prepared by deposition on the front surface (directed to the edge of the rotary table as plate 0°), and the other batch could be prepared by deposition on the rear surface (directed to the center of the rotary table as plate 180°). In addition, the holder was affixed at 90° and 45° in relation to the cathode, as plate 90° and plate 45°, respectively.

Preparation of the specimens included cleaning in pulsed Ar glow discharge at 425 °C, with a bias of −850 V at a pressure of  $4 \times 10^{-3}$  mbar (0.4 Pa) to reduce the volume of contaminants and oxides on the deposited surface of the specimens. After that, a thin metallic pure Ti layer (Ti etching) was deposited in an Ar environment to create a valuable adhesion layer on the surface of the substrate. The top coating was deposited onto the adhesion (buffer) layer, with a thickness of about 300 nm, which was deposited directly onto the substrate with the same parameters as those of the top layer.

After measuring the length variation in the coated tube and the deflection of the coated plate, three pieces were cut from one tube (two from the ends and one from the middle) with a length of 10 mm, and two pieces were cut from the plates with differing depositing positions, with dimensions of 10 mm  $\times$  10 mm, for SEM analysis.

By means of the use of Field Emission Gun Scanning Electron Microscopy (FEGSEM) in Zeiss Ultra-55 HR (SEM- Zeiss, Obercohen, Germany), the microstructure of the coatings was investigated. The coating thicknesses were measured from the SEM images and using the ball-cratering equipment, Calotester kaloMax (BAQ GmbH, Braunschweig, Germany).

The mean values of residual stresses in the coatings were calculated from the length change in the tubular substrate. The calculation formula was presented in our earlier papers [11,16]. As the coating

was relatively thin, it was assumed that residual stresses were distributed uniformly throughout the coating thickness:

$$\sigma = \frac{2E_1}{2(1-\mu_1)d_1} \left( \frac{d_1^2 - d_2^2}{4l} \right) \frac{\Delta l}{h_2}, \quad (1)$$

where  $E_1$  and  $\mu_1$  are the modulus of elasticity and Poisson's ratio of the substrate, respectively, while  $d_1$  is the outer diameter of the tube,  $d_2$  is the inner diameter of the tube,  $h_2$  is the thickness of the coating,  $l$  is the length of the tube, and  $\Delta l$  is the measured length variation in the tube.

From the deflection of the plate, residual stresses were determined using an equation that was based on Stoney's formula [17], but appropriately modified for a plate substrate by introducing the factor  $1/(1-\mu_1)$  to account for the biaxial state of stress [12]:

$$\sigma = \frac{E_1}{6(1-\mu_1)} \frac{t_1^2}{t_2} \kappa, \quad (2)$$

where  $\kappa = (4/b^2)w$  is the curvature of the free surface of the plate substrate as determined via the measured deflection  $w$  in the middle of the coated convex plate;  $t_1$  and  $t_2$  are thicknesses of the substrate and coating respectively; and  $b$  is the coated width.

The unit presented in Figure 2a was adapted from [11] and improved to enable the measurement of the length of the thin walled tubular substrate before and after coating deposition. The measured length variation  $\Delta l$  can be used as an experimental parameter for calculating the average values of residual stresses in coatings.

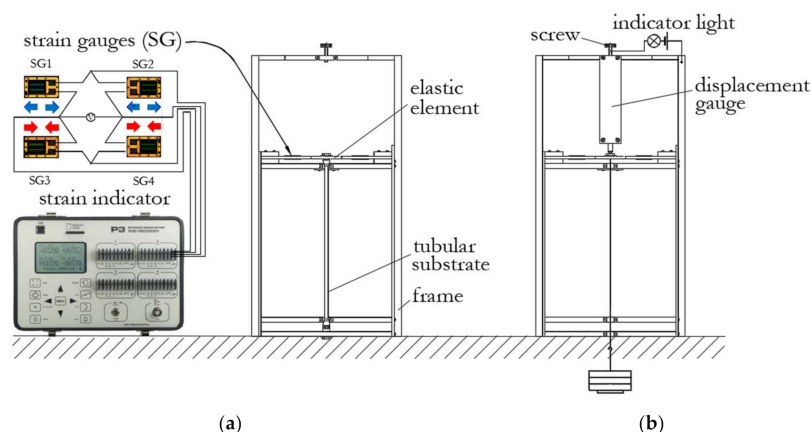


**Figure 2.** The schematic: (a) for the length measuring unit of the tube; (b) for calibration.

The calibration of the length measuring unit is a separate task. The length change in the tubular substrate was transformed to the deformation of the elastic element, which was measured by four strain gauges (Figure 2a). The schematic for the calibration work is presented in Figure 2b. The displacement of the middle cross-section of the elastic element, depending upon the units of the strain indicator in the case of unloading, is presented in Figure 3. During the process of calibration, the readings were taken at a point in time at which rotation of the screw turned off the indicator light.

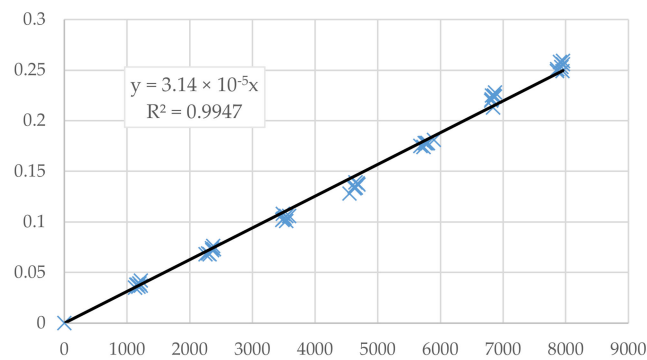


**Figure 3.** The dependence of the strain indicator units on the deflection in the case of unloading.

The constant should be determined so that the relation is approximated in the best way possible by minimizing the square of error; by using the software, MS Excel 2016, this was found by using the regression analysis function. As a result, a constant of  $3.14 \times 10^{-5}$  mm per unit of the strain indicator was obtained. A constant of  $8.26 \times 10^{-5}$  mm per unit was also used before modifications were carried out on the length measuring unit [11]. The modified unit has 2.63 times higher sensitivity levels.

The length of the tube was measured a total of ten times before and ten times after deposition, and the mean value was used to calculate residual stresses in the coating. To guarantee the centering of the tube in the length measuring unit, the inner circular line of the cross section of its ends remained in contact with the spherical surface of the support [11].

### 3. Results

The chemical composition of the coatings was measured using energy dispersive X-ray spectroscopy (EDS) in a Bruker Esprit 1.82 system, and the deposition parameters are presented in Table 2.

**Table 2.** Chemical composition of the coatings (measured and norm) and the deposition parameters.

| Coating | Ti    | Al    | N     | Cr    | Si   | C    | Fe  | Temp<br>T, °C | Pressure,<br>Pa | N <sub>2</sub><br>sccm | C <sub>2</sub> H <sub>2</sub> | Bias Volt.<br>U <sub>b</sub> , V |
|---------|-------|-------|-------|-------|------|------|-----|---------------|-----------------|------------------------|-------------------------------|----------------------------------|
|         |       |       |       | %     |      |      |     |               |                 |                        |                               |                                  |
| nACRo   |       | 19.00 | 27.30 | 43.90 | 2.90 |      | 0.4 | 461           | 1.80            | 147                    |                               | 53                               |
|         |       | 20.35 | 29.18 | 46.90 | 3.12 |      |     |               |                 |                        |                               |                                  |
| AlCrN   |       | 22.80 | 28.10 | 44.60 |      |      |     | 461           | 3.80            | 155                    |                               | 41                               |
|         |       | 23.84 | 29.46 | 46.70 |      |      |     |               |                 |                        |                               |                                  |
| nACo    | 55.40 | 13.60 | 31.30 | 1.30  | 2.40 |      | 0.5 | 476           | 1.32            | 110                    |                               | 76                               |
|         | 53.02 | 13.06 | 29.96 | 1.24  | 2.28 |      |     |               |                 |                        |                               |                                  |
| TiAlN   | 48.10 | 20.60 | 29.50 |       |      |      |     | 450           | 1.30            | 110                    |                               | 62                               |
|         | 48.99 | 20.97 | 30.03 |       |      |      |     |               |                 |                        |                               |                                  |
| TiCN    | 70.80 |       | 28.90 |       |      | 2.80 |     | 450           | 0.49            | 45                     | 5                             | 61                               |
|         | 69.10 |       | 28.20 |       |      | 2.70 |     |               |                 |                        |                               |                                  |

From the results, it is obvious that the thicknesses of those coatings that were deposited on the tubular substrates and the thicknesses of those coatings that were deposited on the plates are significantly different, as they are located at different angles in relation to the cathode. This can be manipulated with the energy of evaporated ions, and hence directly influence the dynamics of growth for the coatings.

The microstructure of the coating on the tube and on the plate was investigated by means of SEM, and the images of the coating's cross-sections and thicknesses are presented in Figures 4 and 5.

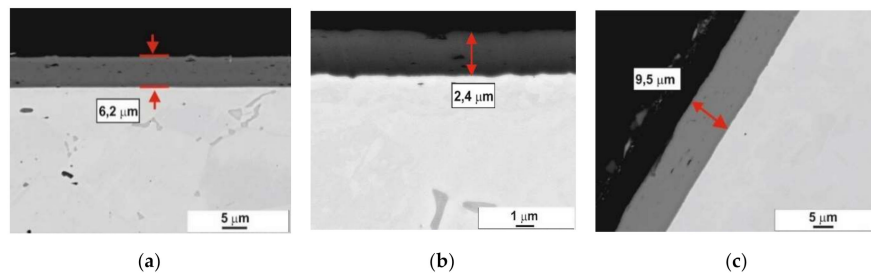


**Figure 4.** SEM of the cross-sections of nACRo coatings applied on the plate and placed: (a) at 180° to the cathode; (b) on the plate placed at 0° to the cathode; and (c) on the tube.

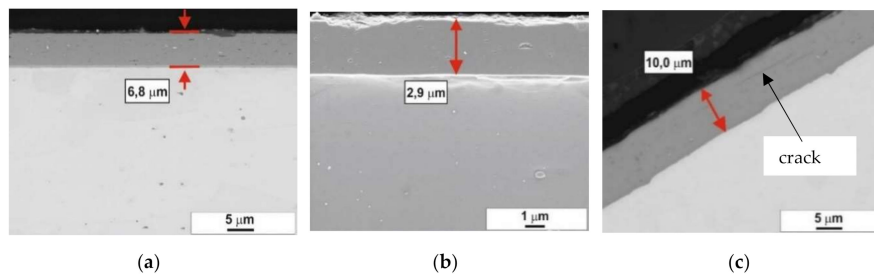


**Figure 5.** SEM of the cross-sections of nACRo coatings applied on the plate and placed: (a) at 180° to the cathode; (b) on the plate placed at 0° to the cathode; and (c) on the tube.

The coating that was deposited on the tube is thicker (Figures 4c and 5c) than the one on the plate, as some part of its surface is constantly forehead-bombarded with target plasma atoms and ions.

It can be seen that coatings on the plates which were directed towards the edge of the rotary table (Figures 4a and 5a) are thicker when they are compared to plates that were directed to the center of the rotary table (Figures 4b and 5b). This is due to the minimal potential distance between the target and the substrate, as well as the larger parameters of kinetic energy during deposition. The coated surface of the plate is directly orientated towards the cathode and is bombarded with atoms, ions, and metal-rich microparticles.

In the case of the plates that were directed towards the center of the rotary table, the potential distance between the target and the substrate is at its maximum and the parameters for kinetic energy during deposition are smaller, and, consequently, the thickness of the coating is less (Figures 4b and 5b) when compared to those plates that were directed towards the edge of the rotary table.

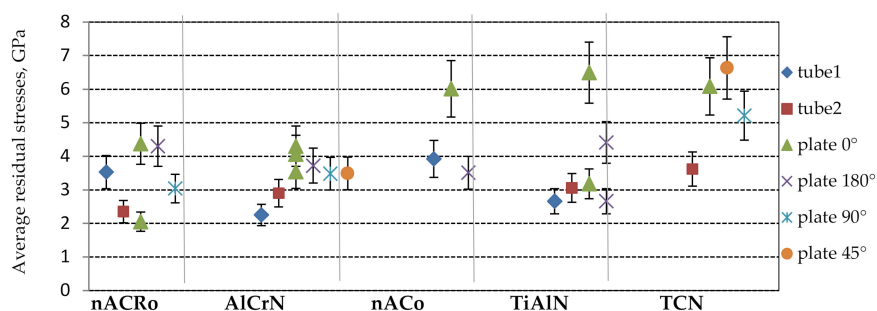
By using direct measurements of the layer's thicknesses from SEM images and the ball-cratering equipment, Kalotester KaloMax, the average values of residual stresses were calculated by means of Equations (1) and (2), as presented in Table 3.

**Table 3.** Coating type, substrate dimensions, and coating thickness, with average residual stresses in the coatings.

| Coating Type | Placement of Plates,<br>Mean Values of<br>Substrate Dimensions,<br>mm | Mean<br>Coating<br>Thickness,<br>$\mu\text{m}$ | Average Residual Stresses, GPa |                  |   |
|--------------|---|--|--------------------------------|------------------|---|
|              |   |  | Calculation Result             |                  | Literature<br>X-ray<br>Technique                |
|              |   |  | Equation (1)                   | Equation (2)     |   |
| nACRo        | Gradient<br>(nanocomposite)   | plate $0^\circ$ $t_1 = 0.241$ *                |                                | $-2.05 \pm 0.20$ | $-5.2$ [18]<br>$t_2 = 2.3 \mu\text{m}$          |
|              |   | plate $90^\circ$ $0.243$ *                     |                                | $-3.04 \pm 0.33$ |   |
|              |   | tube 2   | $-2.35 \pm 0.37$               |                  |   |
|              |   | plate $0^\circ$ $0.315$                        |                                | $-4.37 \pm 0.68$ |   |
|              |   | plate $180^\circ$ $0.314$                      |                                | $-4.30 \pm 0.60$ |   |
|              |   | tube 1   | $-3.53 \pm 0.43$               |                  |   |
| AlCrN        | Gradient<br>multilayer  | plate $0^\circ$ $0.484$                        |                                | $-4.30 \pm 0.79$ | $-4.9$ [19]<br>$-4.0$ [18]<br>$3.2 \mu\text{m}$ |
|              |   | plate $0^\circ$ $0.395$ *                      |                                | $-3.54 \pm 0.77$ |   |
|              |   | plate $45^\circ$ $0.394$ *                     |                                | $-3.49 \pm 0.61$ |   |
|              |   | plate $90^\circ$ $0.393$ *                     |                                | $-3.48 \pm 0.73$ |   |
|              |   | tube 2   | $-2.90 \pm 0.10$               |                  |   |
|              |   | plate $0^\circ$ $0.306$                        |                                | $-4.06 \pm 0.30$ |   |
|              |   | plate $180^\circ$ $0.308$                      |                                | $-3.72 \pm 0.99$ |   |
| nACo         | Multilayer<br>(nanocomposite)<br>Hard grade                           | plate $0^\circ$ $0.315$                        |                                | $-6.01 \pm 0.66$ | $-4.8$ [18]<br>$2.8 \mu\text{m}$                |
|              |   | plate $180^\circ$ $0.311$                      |                                | $-3.51 \pm 0.94$ |   |
|              |   | tube 1   | $-3.92 \pm 0.09$               |                  |   |
| TiAlN        | Multilayer  | plate $0^\circ$ $0.395$                        |                                | $-6.49 \pm 0.36$ | $-5.7$ [20]<br>$-(6.3-7.5)$<br>[21]             |
|              |   | plate $180^\circ$ $0.395$                      |                                | $-4.41 \pm 0.28$ |   |
|              |   | tube 2   | $-3.06 \pm 0.15$               |                  |   |
|              |   | plate $0^\circ$ $0.244$                        |                                | $-3.18 \pm 0.19$ |   |
|              |   | plate $180^\circ$ $0.244$                      |                                | $-2.66 \pm 0.37$ |   |
| TiCN         | Gradient  | tube 1   | $-2.66 \pm 0.26$               |                  | $-(4.6-5.0)$<br>[22]                            |
|              |   | plate $0^\circ$ $0.397$                        |                                | $-6.08 \pm 0.36$ |   |
|              |   | plate $45^\circ$ $0.393$ *                     |                                | $-6.63 \pm 0.36$ |   |
|              |   | plate $90^\circ$ $0.393$ *                     |                                | $-5.21 \pm 0.59$ |   |
|              |   | tube 2   | $-3.62 \pm 0.10$               |                  |   |

\* Test samples were coated in separate runs: Tube 1,  $3.0 \text{ mm} \times 2.70 \text{ mm} \times 167.37 \text{ mm}$ ; Tube 2,  $3.0 \text{ mm} \times 2.50 \text{ mm} \times 167.57 \text{ mm}$ .

To gain a better overview of the measured residual stresses for different types of coatings, a graph is presented in Figure 6.

**Figure 6.** Average residual stresses depending on the type of coatings, and the form and affixing orientation of the substrates in relation to the cathode.

The shape of the substrate's surface and the orientation of the coated surface in relation to the cathode have an effect on average residual stresses in the coatings. It can be noted that the content of Si does not affect residual stresses. Residual stresses in Ti-containing coatings are higher than those in Cr-containing coatings, and this trend is evident for coatings that have been deposited on the plate's front surface. In our experiments, the orientation of the coated surface towards the cathode did



not have an effect on residual stresses in the TiCN coatings. The average residual stresses that were obtained fall within the range that is presented in the available literature, where the X-ray technique is mainly used for the measurement of residual stresses. Such good agreement between residual stresses that have been obtained by physically different methods can be explained by the microstructure of the coatings that were investigated. It should also be noted that the proportions of the chemical composition elements in the compared coatings may differ slightly.

#### 4. Discussion

The authors of [14] stated that compression stresses in a coating usually lead to the formation of delamination and longitudinal cracks. Cracks in coatings are a critical property in wear resistance. If a failure of the coating occurs during the working state (residual compressive stresses are summarized with contact stresses), the coating's capabilities can be greatly reduced, which causes severe abrasion that in turn can place wear on the friction system (pair of friction). Cracks were observed in two nanocomposite nACRo and nACo coatings on the cylindrical substrate and at the deposition parameters used in this study. Stress-induced cracks were found to be perpendicular to the direction of growth (Figure 5c), and we assume that cracking leads to a relaxation of the stress that is accumulated in the growing coating during deposition and a decline in overall residual stresses. The reason for cracking can be related to the plain state of compressive stress, which induces stresses in the radial direction of the coating. Radial stress in the interface of the substrate and coating can be calculated according to Equation (3) that is presented in [23]:

$$\sigma_r = \frac{\sigma h_2}{r_1 + h_2}. \quad (3)$$

For example, as the nACo hard grade coating has  $h_2 = 9.5 \mu\text{m}$ ,  $\sigma = -3.92 \text{ GPa}$ , and  $r_1 = 1.5 \text{ mm}$ ,  $\sigma_r = 26.2 \text{ MPa}$ , which is considerable (the ultimate tensile strength of the coating is unknown). When the same coating is placed on a cylindrical surface with  $r_1 = 10 \text{ mm}$ ,  $\sigma_r = 3.72 \text{ MPa}$ ; when it is on a spherical surface with  $r_1 = 2.5 \text{ mm}$ ,  $\sigma_r = 14.8 \text{ MPa}$  [24]. It is evident that, when the radius of the substrate increases, residual stresses decrease in a linear fashion.

There were no visible cracks in coatings that were deposited on the plate substrate and in those coatings that were deposited on the tube substrate: AlCrN with a thickness of  $7.1 \mu\text{m}$  and TiCN with a thickness of  $8.8 \mu\text{m}$ .

In industrial field wear tests with fine-blanking punches (using a convex surface), the three PVD coatings TiCN, nACRo, and nACo were estimated to have average coating relative wear ( $w_i$ ) values of 84.3%, 66.7%, and 69.9%, correspondingly [24]. TiCN coating wear was 15–17% higher than that of nACRo and nACo coatings, but it is difficult to find any differences between those two [24]. The average residual stresses obtained in coatings on different substrates (Table 3) were  $-5.39 \text{ MPa}$  for TiCN,  $-3.27 \text{ MPa}$  for nACRo, and  $-4.48 \text{ MPa}$  for nACo.

It can be concluded that the higher average residual compressive stress in the coating correlates to the higher average relative wear resistance levels during industrial field wear testing. There is a dependence of the elastic strain towards a failure parameter (the hardness to modulus of the elasticity ratio or  $H/E$ ) in terms of the measured coating average relative wear for industrial tests, meaning that the same correlation stands for residual stresses that were measured in the same coatings systems. The combination of the highest  $H/E$  ratio and lowest compressive residual stress leads to the lowest relative wear (or higher wear resistance), as proven by the superior behavior of the nACo coating in the industrial field wear testing process. However, the difference between the wear behavior in nACo and nACRo coatings is quite insignificant, as the mechanical properties are quite similar.

The same tendencies can be seen in the indentational response of the coating systems being studied, along with impact wear and indentation surface fatigue behavior [25–27]. The nACo and nACRo coatings reveal lower coating failed area ratios (FR, %) when they are compared to TiCN, at a level of 24–42% for  $10^3$  and  $5 \times 10^6$  for the of impact figures, respectively [27]. The FR for TiCN for the same impact figure range is 31–45%. This conclusion is valid for different forms of substrates [26].



The nACo behavior is still superior to that of the TiCN, independent of the variation of the hard metal or cermet substrate composition.

## 5. Conclusions

The average residual stresses in various PVD hard coatings on tube and plate substrates were calculated using as an experimental parameter, along with the length variation of the tube, and the deflection of the plate. The major conclusions are summarized as follows:

The length measuring unit was improved to make possible the measurement of the length of the thin-walled tubular substrate before and after coating deposition.

The calculated average values of residual stresses were compressive and high, varying from 2.05 to 6.63 GPa, and were of the same range as the corresponding data shown in the available literature that were obtained by the X-ray technique.

The coating deposited on the tube substrate was thicker, and average residual stresses in it were lower than that of coatings on plate substrate. Residual stresses were at their highest in the coating that were deposited on the front surface of the plate; the values for residual stresses on those plates that were inclined (45°) and perpendicular (90°) with respect to the cathode were within the same range.

The microstructure of the coating on the tube and on the plate was investigated by means of SEM, and the images of the coating's cross-sections and thicknesses are presented. Observed cracks were perpendicular to the direction of growth in the nanocomposite nACRo and nACo coatings which were deposited on the tube substrate.

The combination of the highest levels of hardness to the modulus of the elasticity ratio (H/E or elastic strain to failure) and the lowest average residual stress levels is proven to have a positive effect on the wear resistance and indentational (cyclic impact loading) behavior of the coatings. The nACo and nACRo coatings systems showed a tendency to be superior over other studied coatings, with a wear resistance during industrial trials of 15–17% higher than that of TiCN and a lower coating failure ratio (FR) of around 10% for cyclic loading of up to  $5 \times 10^6$  cycles.

The presented analysis is limited to the data that were obtained from the aforementioned experiments.

**Author Contributions:** Conceptualization, H.L.; methodology, H.L. and A.R.; software, V.M.; validation, H.L. and F.S.; formal analysis, P.P.; investigation, H.L., A.R., and L.L.; data curation, H.L., L.L., and F.S.; writing—original draft preparation, H.L.; writing—review and editing, A.R. and F.S.; visualization, H.L. and A.R.; supervision, J.K.; and funding acquisition, J.K. All authors have read and agreed to the published version of the manuscript.

**Funding:** This research was supported by the institutional research funding project, “Multi-scale structured ceramic-based composites for extreme applications” (IUT 19–29), and by the grant, “Composites ‘ceramics-Fe alloy’ for a wide range of application conditions” (PRG665), of the Estonian Research Council. The financial support from the Tallinn University of Technology is highly appreciated (a targeted grant for the “Metals Processing professorship”).

**Acknowledgments:** The authors are thankful to Eron Adoberg and Heinar Vagiström from Tallinn University of Technology for their technical support. The authors are also thankful to the European Union through the European Regional Development Fund, Project TK141.

**Conflicts of Interest:** The authors declare no conflict of interest.

## References

1. Gonzalo, O.; Navas, V.G.; Coto, B.; Bengoetxea, I.; de Gopegi, U.R.; Etxaniz, M. Influence of the coating residual stresses on the tool wear. *Proc. Eng.* **2011**, *19*, 106–111. [CrossRef]
2. Quinto, D.T. Twenty-five years of PVD coatings at the cutting edge. *Fall Bull.* **2007**, 17–22. Available online: [https://www.svc.org/DigitalLibrary/documents/2007\\_Fall\\_DTQ.pdf](https://www.svc.org/DigitalLibrary/documents/2007_Fall_DTQ.pdf) (accessed on 28 October 2020).
3. Kumar, T.S.; Prabu, S.B.; Manivasagam, G.; Padmanabhan, K.A. Comparison of TiAlN, AlCrN and AlCrN/TiAlN coatings for cutting-tool applications. *Int. J. Min. Met. Mater.* **2014**, *21*, 796–805. [CrossRef]
4. Koch, R. Stress in Evaporated and Sputtered Thin Films—A Comparison. *Surf. Coat. Technol.* **2010**, *204*, 1973–1982. [CrossRef]

5. Soroka, O.B. Evaluation of residual stresses in PVD-coatings. Part 1. Review. *Strength Mater.* **2010**, *42*, 287–296. [CrossRef]
6. Soroka, O.B. Evaluation of residual stresses in PVD-coatings. Part 2. *Strength Mater.* **2010**, *42*, 450–458. [CrossRef]
7. Lu, J. *Handbook of Measurement of Residual Stresses*, 1st ed.; Fairmont Press: Upper Saddle River, NJ, USA, 1996; p. 253.
8. Kandil, F.A.; Lord, J.D.; Fry, A.T.; Grant, P.V. A Review of Residual Stress Measurement Methods—A Guide to Technique Selection. NPL Report MATC (A) 2001, 04. Available online: <https://eprintspublications.npl.co.uk/1873/1/malc4.pdf> (accessed on 28 October 2020).
9. Abadias, G.; Chason, E.; Keckes, J.; Sebastiani, M.; Thompson, G.; Barthel, E.; Doll, G.; Murray, C.; Stoessel, C.; Martinu, L. Review Article: Stress in thin films and coatings: Current status, challenges, and prospects. *J. Vac. Sci. Technol.* **2018**, *36*, 020801. [CrossRef]
10. Lille, H.; Kõo, J.; Gregor, A.; Ryabchikov, A.; Sergejev, F.; Traksmas, R.; Kulu, P. Comparison of Curvature and X-Ray Methods for Measuring of Residual Stresses in Hard PVD Coatings. *Mater. Sci. Forum* **2011**, *681*, 455–460. [CrossRef]
11. Lille, H.; Ryabchikov, A.; Kõo, J.; Adoberg, E.; Mikli, V.; Kübarsepp, J.; Peetsalu, P. Evaluation of Residual Stresses in PVD Coatings by means of Tubular Substrate Length Variation. *Mater. Res. Proc.* **2018**, *6*, 131–136. [CrossRef]
12. Lille, H.; Ryabchikov, A.; Kõo, J.; Adoberg, E.; Lind, L.; Kurisoo, L.; Peetsalu, P. Evaluation of Residual Stresses in PVD Coatings by Means of Strip Substrate Length Variation and Curvature Method of Plate Substrate. *Solid State Phenom.* **2017**, *267*, 212–218. [CrossRef]
13. The Advantages of PVD Coating for Cutting Tools. Available online: <http://www.pvdtarget.com/info/the-advantages-of-pvd-coating-for-cutting-tool-23249873.html> (accessed on 28 October 2020).
14. Vereschaka, A.; Volosova, M.; Chigarev, A.; Sitnikov, N.; Ashmarin, A.; Sotova, C.; Bublikov, J.; Lytkin, D. Influence of the Thickness of a Nanolayer Composite Coating on Values of Residual Stress and the Nature of Coating Wear. *Coatings* **2020**, *10*, 63. [CrossRef]
15. Sprute, T.; Tillmann, W.; Grisales, D.; Selvadurai, U.; Fischer, G. Influence of substrate pre-treatments on residual stresses and tribo-mechanical properties of TiAlN-based PVD coatings. *Surf. Coat. Technol.* **2014**, *260*, 369–379. [CrossRef]
16. Kõo, J.; Ryabchikov, A. On the determination of residual stresses in coatings from measured longitudinal deformation of a wire substrate. In Proceedings of the 19th Symposium on Experimental Mechanics of Solids, Jachranka, Poland, 18–20 October 2000; Stupinicki, J., Ed.; Warsaw University of Technology: Jachranka, Poland, 2000; pp. 319–324. Available online: <http://hdl.handle.net/10492/3803> (accessed on 28 October 2020).
17. Kõo, J.; Valgur, J. Residual stress measurement in coated plates using layer growing/removing methods: 100th anniversary of the publication of Stoney’s paper “The tension of metallic films deposited by electrolysis”. *Mater. Sci. Forum* **2011**, *681*, 165–170. [CrossRef]
18. Paiva, J.M.; Fox-Rabinovich, G.; Locks, E., Jr.; Stolf, P.; Seid Ahmed, Y.; Matos Martins, M.; Veldhuis, S. Tribological and Wear Performance of Nanocomposite PVD Hard Coatings Deposited on Aluminium Die Casting Tool. *Materials* **2018**, *11*, 358. Available online: <https://www.ncbi.nlm.nih.gov/pmc/articles/PMC5872937/> (accessed on 28 October 2020).
19. Haršáni, M.; Ghafoor, N.; Calamba, K.; Žáčková, P.; Sahul, M.; Vopát, T.; Satrapinskyy, L.; Čaplovicová, M.; Čaplovič, L. Adhesive-deformation relationships and mechanical properties of nc-AlCrN/a-SiNx hard coatings deposited at different bias voltages. *Thin Solid Film.* **2018**, *650*, 11–19. [CrossRef]
20. Skordaris, G.; Bouzakis, K.; Kotsanis, T.; Charalampous, P.; Bouzakis, E.; Breidenstein, B.; Bergmann, B.; Denkena, B. Effect of PVD film’s residual stresses on their mechanical properties, brittleness, adhesion and cutting performance of coated tools. *CIRP J. Manuf. Sci. Technol.* **2017**, *18*, 145–151. [CrossRef]
21. Chang, Y.-Y.; Wang, D.-Y. Characterization of nanocrystalline AlTiN coatings synthesized by a cathodic-arc deposition process. *Surf. Coat. Technol.* **2007**, *201*, 6699–6701. Available online: <https://www.sciencedirect.com/science/article/pii/S0257897206010437> (accessed on 28 October 2020).
22. Murotani, T.; Hirose, H.; Sasaki, T.; Okazaki, K. Study on stress measurement of PVD-coatings layer. *Thin Solid Film.* **2000**, *377–378*, 617–620. [CrossRef]
23. Ryabchikov, A. Development of Some Mechanical Methods for Measurement of Residual Stresses in Coatings. Ph.D. Thesis, Estonian University of Life Sciences, Tartu, Estonia, 2005.

24. Lind, L.; Peetsalu, P.; Sergejev, F. Wear of Different PVD Coatings at Industrial Fine-blanking Field Tests. *Mater. Sci. (Medžiagotyra)* **2015**, *21*, 343–348. [[CrossRef](#)]
25. Sivitski, A.; Gregor, A.; Saarna, M.; Kulu, P.; Sergejev, F. Properties and performance of hard coatings on tool steels under cyclic indentation. *Acta Mech. Slovaca* **2009**, *13*, 84–95. Available online: <https://www.actamechanica.sk/pdfs/ams/2009/03/10.pdf> (accessed on 28 October 2020).
26. Veinthal, R.; Sergejev, F.; Yaldiz, C.E.; Mikli, V. Impact Wear Performance of Thin Hard Coatings on TiC Cermets. *J. ASTM Int.* **2011**, *8*, 103272. [[CrossRef](#)]
27. Antonov, M.; Hussainova, I.; Kulu, P.; Sergejev, F.; Gregor, A. Assessment of gradient and nanogradient PVD coatings behaviour under erosive, abrasive and impact wear conditions. *Wear* **2009**, *267*, 898–906. [[CrossRef](#)]

**Publisher's Note:** MDPI stays neutral with regard to jurisdictional claims in published maps and institutional affiliations.



© 2020 by the authors. Licensee MDPI, Basel, Switzerland. This article is an open access article distributed under the terms and conditions of the Creative Commons Attribution (CC BY) license (<http://creativecommons.org/licenses/by/4.0/>).